



ORBITAL MECHANICS ASSIGNMENT

INTERPLANETARY & PLANETARY PRELIMINARY MISSION ANALYSIS

Academic Year 2023/2024

Group ID: **2304**

Authors:

Aufiero	Luca	10530771
Caushi	Andrea	10611148
Luciardello Lecardi	Matteo	10572870

Person code:

Supervisors:

C. Colombo
J.L. Gonzalo Gomez

January 2024

Contents

1 Interplanetary Explorer Mission	1
1.1 Time constraints on departure and arrival	1
1.2 Design strategy	1
1.2.1 Optimization phase and results	3
1.2.2 Interplanetary trajectory characterization	5
2 Planetary Explorer Mission	8
2.1 Ground track	8
2.1.1 Repeating ground track	9
2.2 Orbit propagation	10
2.3 Filtering of high frequencies	12
2.4 Comparison with real data	13

1 Interplanetary Explorer Mission

The PoliMi Space Agency is carrying out a feasibility study for a potential Interplanetary Explorer Mission visiting the Near Earth Asteroid (NEO-81) 2005EL70, with an intermediate fly-by on Venus and departure from Mercury. The team is requested to analyze and study the different transfer options and propose a solution based on the mission cost (measured through total Δv).

1.1 Time constraints on departure and arrival

The mission is constrained with a time window of 30 years:

- **Earliest possible departure date from Mercury:** 01/01/2028 00:00:00
- **Latest possible arrival date at NEO-81:** 01/01/2058 00:00:00

1.2 Design strategy

The design of the interplanetary transfer will use the "patched conics" method, therefore studying two Lambert's arcs from Mercury to Venus and from Venus to NEO-81 2005EL70. In addition, the initial and final heliocentric orbits of the spacecraft will be considered respectively equal to the orbit of the departure and arrival body.

The design process starts with a proper selection of the time windows in which the analysis is conducted. Given the initial time window provided as constraint is 30 years long, studying this whole interval would meaninglessly increase the computational cost, therefore a way to reduce this time window into a smaller one is needed.

To achieve this, the orbital and synodic periods (for pairs of bodies) have been computed, so to implement a numerical calculation of an approximated synodic period between the 3 bodies, following this algorithm [1]. The method aims to define a period of configuration repetition, which means that «if the three bodies are initially in a line from one side of the Sun, i.e. closest to each other, after this period they will be "companions" again».

Cosider the orbital periods $P_1 < P_2 < P_3$

Synodic periods:

$$P_{12} = \frac{1}{\frac{1}{P_1} - \frac{1}{P_2}} \quad (1)$$

P_{23} and P_{13} can be similarly obtained.

There is a three-planet resonance if the ratio of the synodic period is a simple integer ratio:

$$\frac{P_{12}}{P_{23}} = \frac{i}{j} \quad (2)$$

Mean motion of bodies: n_1, n_2, n_3 as $n = \sqrt{\frac{\mu_S}{a^3}}$

$$\frac{n_1 - n_2}{n_2 - n_3} = \frac{n_{12}}{n_{23}} \quad (3)$$

If this ratio is > 1 , input $i = 1$, otherwise $j = 1$

The other index is calculated as:

$$j = \text{round} \left[i \frac{n_{12}}{n_{23}} \right] \quad (\text{or calculate } i \text{ from the same equation}) \quad (4)$$



Then, the following quantities are needed:

$$P_{ij} = (i + j) P_{13} \quad (5)$$

$$P'_1 = \frac{i}{(i + j)} - \frac{j}{P_2} - \frac{j}{P_3} \quad (6)$$

$$\Delta P_1 = P'_1 - P_1 \quad (7)$$

Input a new value of the index $i = i + 1$ (or $j = j + 1$) and repeat the previous steps from eq.(4), until the ratio $|\Delta P_1| / P_1 \leq 0.01$ for i and this value is smaller than $|\Delta P_1| / P_1$ for $i + 1$.

As a matter of fact, $T_{syn,123} = P_{ij}$ at i when the mentioned condition is met.

$$T_{syn,123} = 7.513 \text{ years} = 2744.163 \text{ days} \quad (8)$$

Therefore, the whole time window was divided in sub-windows of length $T_{syn,123}$ starting from the earliest departure date, and the study was conducted only on the first one (reported in Table 1), so that the mission could start as soon as possible.

Selected time window	
Earliest departure date	01/01/2028 00:00:00
Latest departure date	07/07/2035 03:54:41

Table 1: Restricted time window selected for the problem

Thus, the preliminary design can be formulated as a constrained parametric optimisation problem with 3 degrees of freedom (DoF) : departure time, flyby time and arrival time. As stated in [2], tackling the problem directly with this approach would result in a cubic $n \times m \times l$ computation effort, where n,m,l are associated to the number of departure, flyby and arrival dates. On the other hand, a rather efficient implementation would study the two Lambert's arcs separately (the provided `lambertMR.m` function was used), therefore splitting the problem into a couple of 2-DoF sub-problems that have 1 DoF in common, i.e. the flyby date, reducing the computational effort back to quadratic plus linear: $n \times m + m \times l$, or $m(n + l)$ number of targeting problems.

Both arcs are studied separately and with the same approach, which consists in implementing a grid-search algorithm to find the Δv of maneuvers for both ends of each arc. In the grid search process, the time step discretization is chosen considering a fraction of the total period of the departure and arrival bodies of the single arc, based on an angle discretization $\Delta\psi$:

$$t_{grid,i} = \frac{\Delta\psi}{360} T_i \quad i = 1, 2 \quad (9)$$

Where T_i is the orbital period of the departure and arrival bodies respectively. A $\Delta\psi = 10^\circ$ was chosen for both windows as initial choice, being relatively fast in term of computational efficiency ($\simeq 20 \text{ min}$).

	$\Delta\psi [\text{deg}]$	$t_{grid} [\text{days}]$
Mercury	10	2.4436
Venus	10	6.2417
NEO-81	10	34.7342

Table 2: Initial grid discretization

Furthermore, a constraint on the time of flight has been imposed for every combination of Lambert's transfers: only arcs characterized by a time of flight that falls between the parabolic time Δt_{par} and the longest orbital period between the two bodies $\max\{T_1; T_2\}$ have been computed.



Consequently, the fly-by date is fixed for every combination of the two arcs, obtaining physical trajectories for the two arcs combined, from departure (Mercury) to arrival (NEO 2005EL70). In addition, the constraint of no impact with Venus is considered, discarding all solutions that would not apply:

$$r_p \geq R_V + h_{atm} \quad (h_{atm} = 500\text{km}) \quad (10)$$

	Date	$\Delta v [\text{km/s}]$
Departure	04/03/2029 12:16:04 UTC	16.101
Fly-by	07/04/2029 02:20:07 UTC	2.226
Arrival	29/03/2032 02:43:02 UTC	8.877
Mission total cost		27.204

Table 3: Result obtained with $\Delta\psi = 10^\circ$

The identical procedure can be replicated by opting for a smaller discretization value, such as $\Delta\psi = 2^\circ$, to further explore the search space and identify additional minima that may not have been detected in the earlier case. This refinement could yield results that are potentially more favorable in terms of total Δv .

	$\Delta\psi [\text{deg}]$	$t_{grid} [\text{days}]$
Mercury	2	0.4887
Venus	2	1.2483
NEO-81	2	6.9468

Table 4: Refined grid discretization

This, however, resulted in an increased computational time, requiring the division of the total time window length $T_{syn,123}$ into several sub-windows to ensure the script's completion within a feasible time frame ($\simeq 7\text{hours}$). This refinement led to the discovery of an improved solution.

	Date	$\Delta v [\text{km/s}]$
Departure	05/03/2029 06:26:22 UTC	16.347
Fly-by	07/04/2029 05:54:39 UTC	1.322
Arrival	15/03/2032 22:08:58 UTC	8.001
Mission total cost		25.670

Table 5: Result obtained with $\Delta\psi = 2^\circ$

1.2.1 Optimization phase and results

In order to perform a further refinement of the solution, *MATLAB fmincon.m* algorithm is used, feeding the non linear constraints:

- $r_{p,flyby} \geq R_{Venus} + h_{atm,Venus}$ where $R_{Venus} = 6051.8\text{ km}$ and $h_{atm,Venus} = 500\text{ km}$
- $r_{p,flyby} \leq R_{SOI,Venus}$ where $R_{SOI,Venus} = 617507.7075\text{ km}$ (at fly-by)

As part of the algorithm, the dates for departure, flyby, and arrival obtained through the grid search are employed as initial guess. Subsequently, the algorithm refines these estimates to derive the final solution for the given problem.

	Date [UTC – MJD2000]	$\Delta v [\text{km/s}]$
Departure	04/03/2029 15:41:02 - 10655.1535 days	16.951
Flyby	06/04/2029 00:08:43 - 10687.5061 days	$9.075 \cdot 10^{-11}$
Arrival	15/03/2032 14:37:51 - 11762.1096 days	8.129
Mission total duration ΔT	1106.9561 [days]	
Mission total cost Δv_{tot}		25.080

Table 6: Final results obtained through fmincon refinement



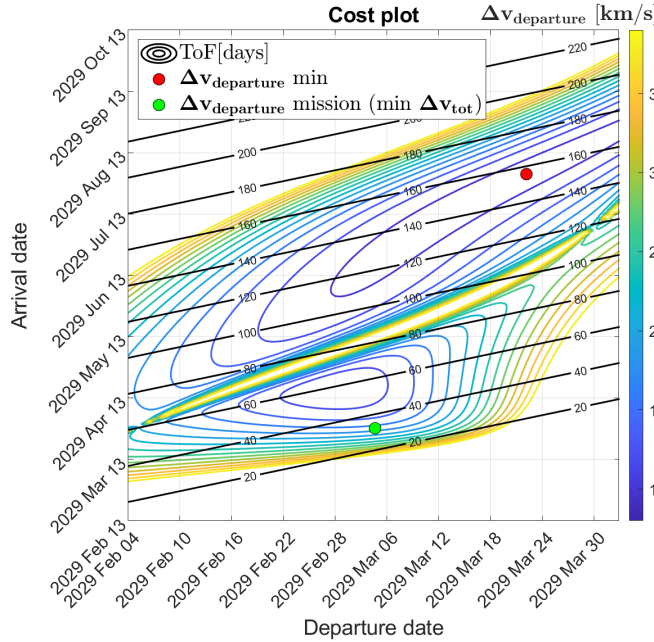


Figure 1: Δv_{dep} Mercury-Venus transfer arc

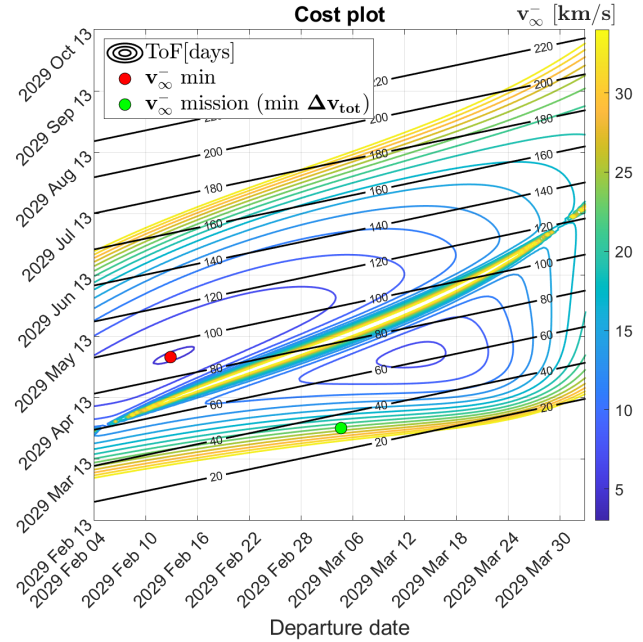


Figure 2: v_∞^- Mercury-Venus transfer arc

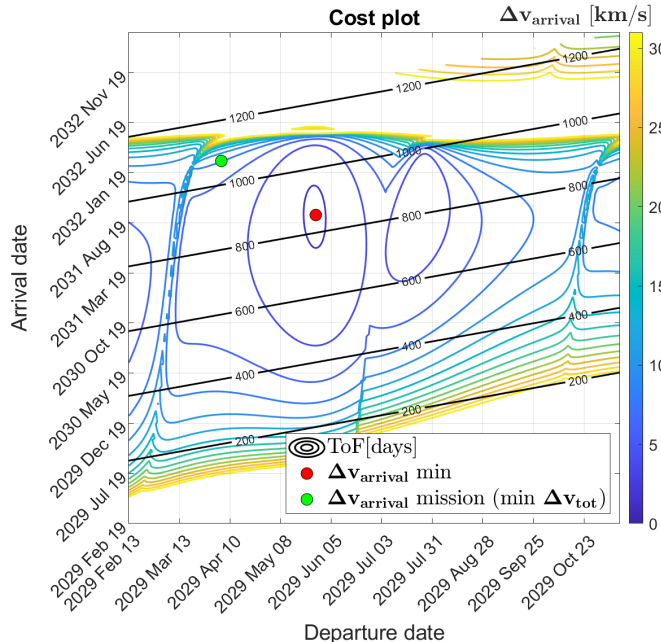


Figure 3: Δv_{arr} Venus-NEO81 transfer arc

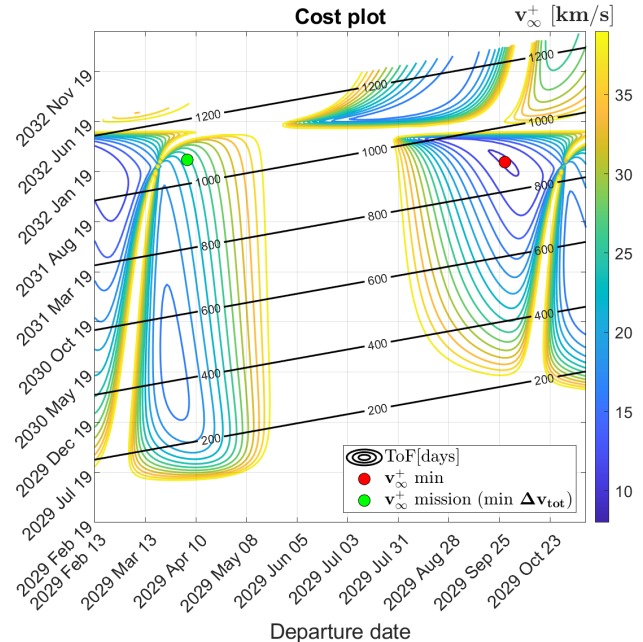


Figure 4: v_∞^+ Venus-NEO81 transfer arc

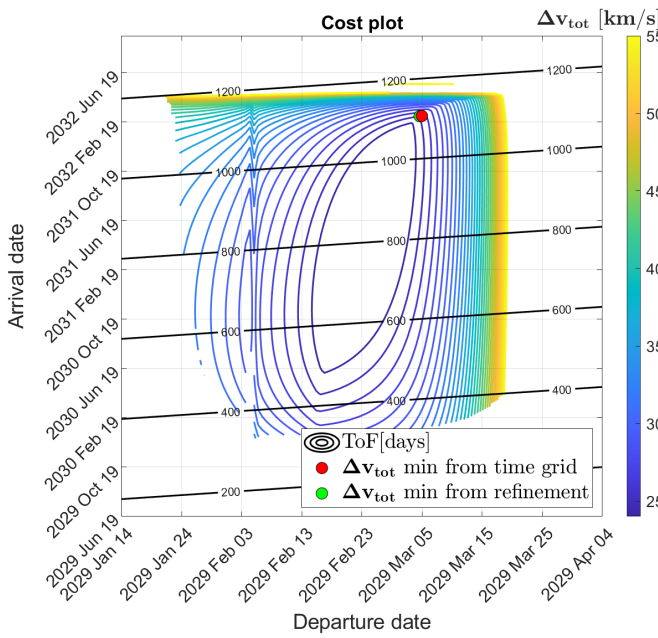


Figure 5: Contour plot Δv_{tot} Mercury-NEO81

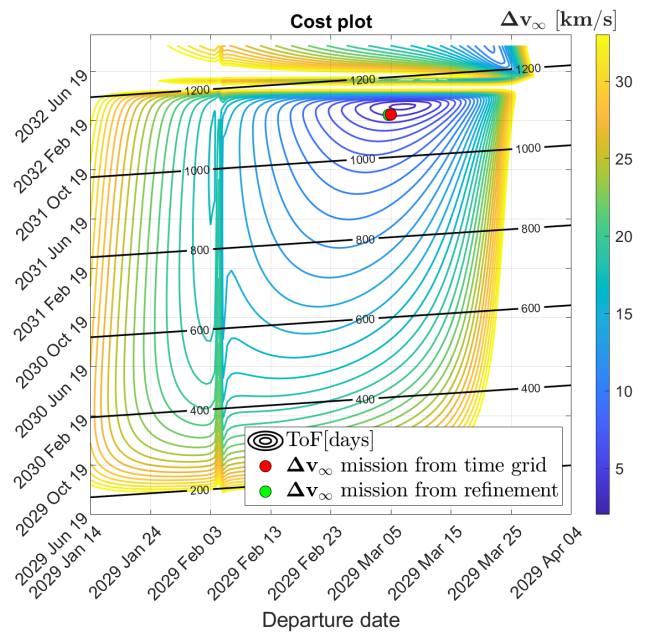


Figure 6: Contour plot Δv_∞ Mercury-NEO81

1.2.2 Interplanetary trajectory characterization

Once the solution from the algorithm was obtained, the chosen transfer arcs can be completely characterized, by the evaluation of the three bodies positions and velocities through `uplanet.m` and `ephNEO.m` ephemerides at the chosen dates.

a [km]	e [-]	i [deg]	Ω [deg]	ω [deg]	θ [deg]	V_1 [km/s]	V_2 [km/s]
$2.0542 \cdot 10^8$	0.6726	6.9003	47.3514	250.1606	347.3051	$\begin{bmatrix} 53.5596 \\ 19.5867 \\ -3.1615 \end{bmatrix}$	$\begin{bmatrix} 6.4690 \\ 41.8563 \\ 2.8560 \end{bmatrix}$

Table 7: Mercury-Venus transfer arc

a [km]	e [-]	i [deg]	Ω [deg]	ω [deg]	θ [deg]	V_1 [km/s]	V_2 [km/s]
$3.3376 \cdot 10^8$	0.7708	4.6570	59.7507	253.5055	71.1306	$\begin{bmatrix} 4.7011 \\ 45.0109 \\ 1.5163 \end{bmatrix}$	$\begin{bmatrix} 18.2228 \\ -14.7207 \\ -1.8864 \end{bmatrix}$

Table 8: Venus-NEO81 transfer arc

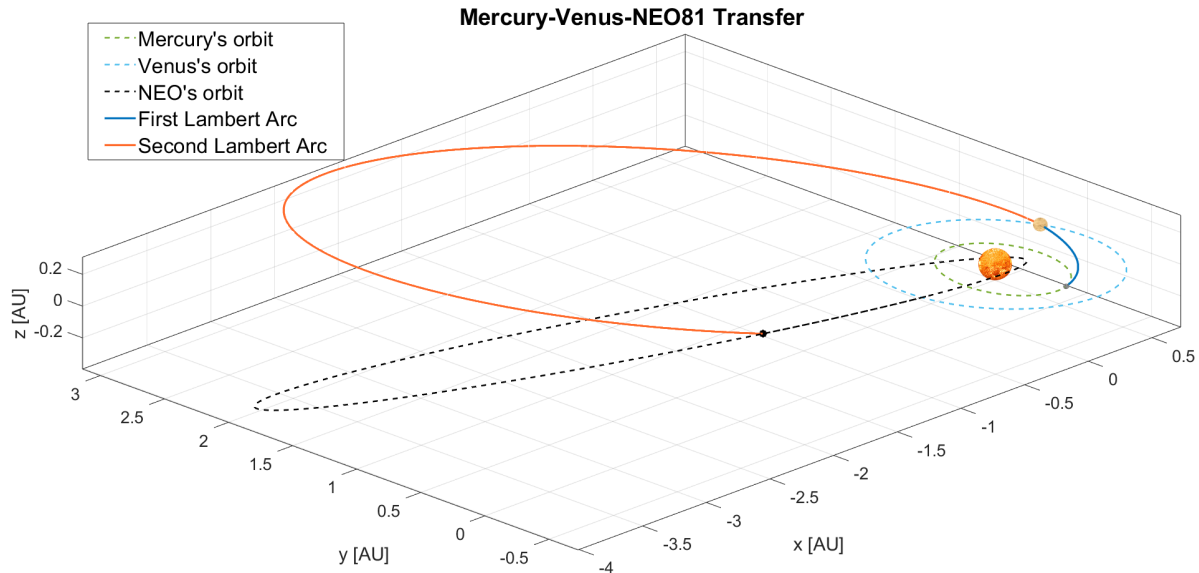


Figure 7: Interplanetary transfer trajectory from Mercury to NEO 2005EL70, 3D view

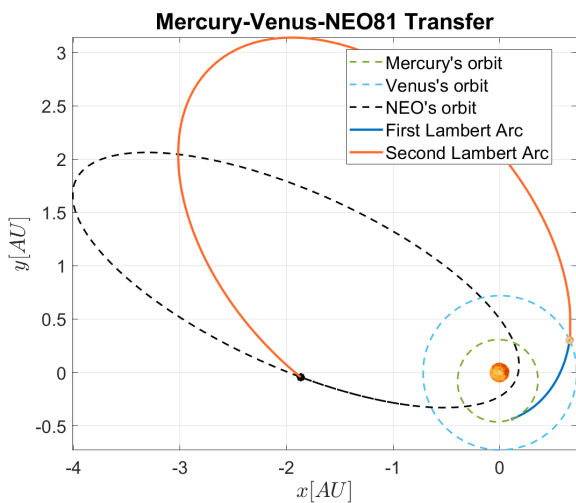


Figure 8: Interplanetary transfer, XY plane

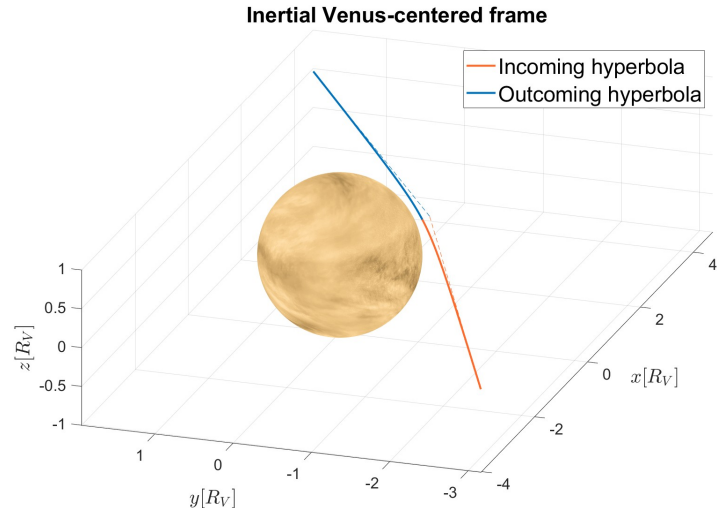


Figure 9: Venus flyby trajectory

The Venus flyby hyperbola can also be fully characterized, starting from the ingoing and outgoing heliocentric velocities of the spacecraft. The constraint for the radius of pericenter is satisfied, obtaining a physical trajectory that does not enter Venus' atmosphere.

$a^- [km]$	$e^- [-]$	$r_p [km]$
-590.5381	12.1639	6592.7263

Table 9: Flyby ingoing hyperbola parameters

$a^+ [km]$	$e^+ [-]$	$r_p [km]$
-590.5381	12.1639	6592.7263

Table 10: Flyby outgoing hyperbola parameters

Moreover, the "fly-by time" can be computed as the duration of the spacecraft flight inside Venus' sphere of influence:

$$\Delta t_{SOI} = 14.568 \text{ hours} \quad (11)$$



The powered gravity assist maneuver at closest approach to Venus (pericenter of fly-by hyperbolic arcs) results being almost negligible. Therefore, the spacecraft would barely consume any fuel, and the optimal fly-by could be considered unpowered, in fact:

$$\Delta v_{pga} = 9.075 \cdot 10^{-11} \text{ km/s} \quad (12)$$

The overall Δv achieved by the fly-by was obtained:

$$\Delta v_{flyby} = 3.856 \text{ km/s} \quad (13)$$

Thus:

$$\frac{\Delta v_{pga}}{\Delta v_{flyby}} = 2.353 \cdot 10^{-11} \quad (14)$$

Finally, the velocity triangles were computed, concluding the fly-by trajectory characterization:

V_V [km/s]	V^+ [km/s]	V^- [km/s]	v_∞^+ [km/s]	v_∞^- [km/s]	Δv [km/s]
$\begin{bmatrix} -14.6222 \\ 31.7197 \\ 1.2701 \end{bmatrix}$	$\begin{bmatrix} 4.7011 \\ 45.0109 \\ 1.5163 \end{bmatrix}$	$\begin{bmatrix} 6.4690 \\ 41.8563 \\ 2.8560 \end{bmatrix}$	$\begin{bmatrix} 19.3233 \\ 13.2912 \\ 0.2462 \end{bmatrix}$	$\begin{bmatrix} 21.0912 \\ 10.1366 \\ 1.5859 \end{bmatrix}$	$\begin{bmatrix} -1.7679 \\ 3.1546 \\ -1.3397 \end{bmatrix}$

Table 11: Velocity triangles for the flyby
Velocity Triangles

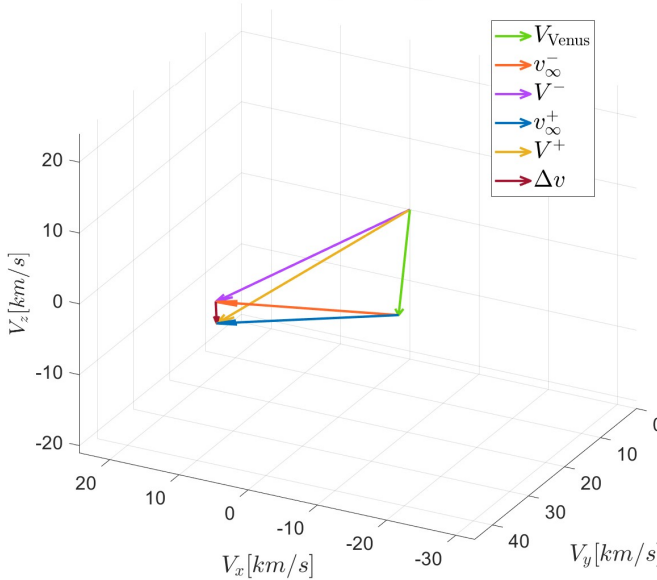


Figure 10: Velocity triangles, 3D view

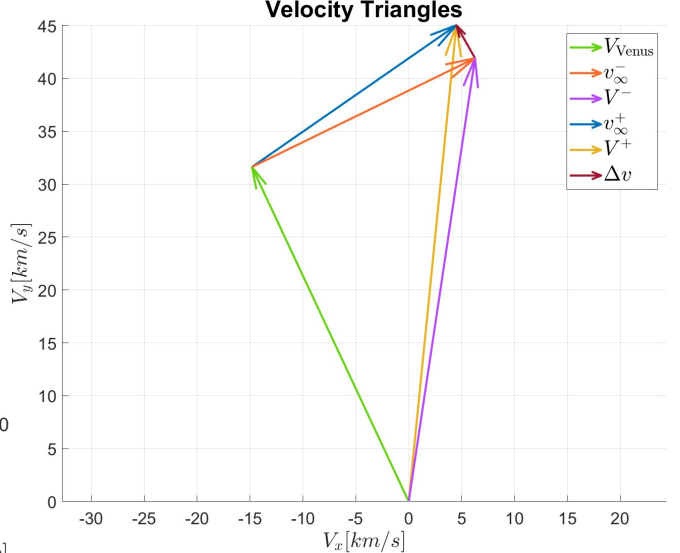


Figure 11: Velocity triangles, XY plane

References

- [1] Borislav Borisov. *Three-planet resonances in the Solar system*. 2011. Astronomical Center, University of Shumen.
- [2] Davide Menzio. “Grid-search applications for trajectory design in presence of flybys”. PhD thesis. 2018/19. Politecnico di Milano.

2 Planetary Explorer Mission

The PoliMi Space Agency wants to launch a Planetary Explorer Mission, to perform Earth observation. This part of the report aims at studying the effect of orbit perturbations (J2 and SRP) on a spacecraft in orbit around the Earth. Two propagation methods are implemented and compared, while frequency analysis is employed to highlight the main harmonics associated with the perturbing effects. The analysis will also dwell on ground track estimation and on an orbit modification to achieve a repeating ground track.

The initial Earth-centered orbit (Figure 17a) is characterized by the following orbital elements:

Table 12: Initial orbital elements

a	e	i	Ω	ω	θ
27251 km	0.4485	11.3122°	0°	0°	0°

The perturbations here accounted for are:

- J_2 effect (i.e. first zonal harmonic), due to Earth's oblateness [1]:

$$\underline{\mathbf{a}}_{J_2} = \frac{3}{2} \frac{J_2 \mu R_\oplus^2}{r^5} \left[\left(5 \frac{z^2}{r^2} - 1 \right) x \hat{\mathbf{i}} + \left(5 \frac{z^2}{r^2} - 1 \right) y \hat{\mathbf{j}} + \left(5 \frac{z^2}{r^2} - 3 \right) z \hat{\mathbf{k}} \right] \quad (15)$$

(where $J_2 = 0.00108263$)

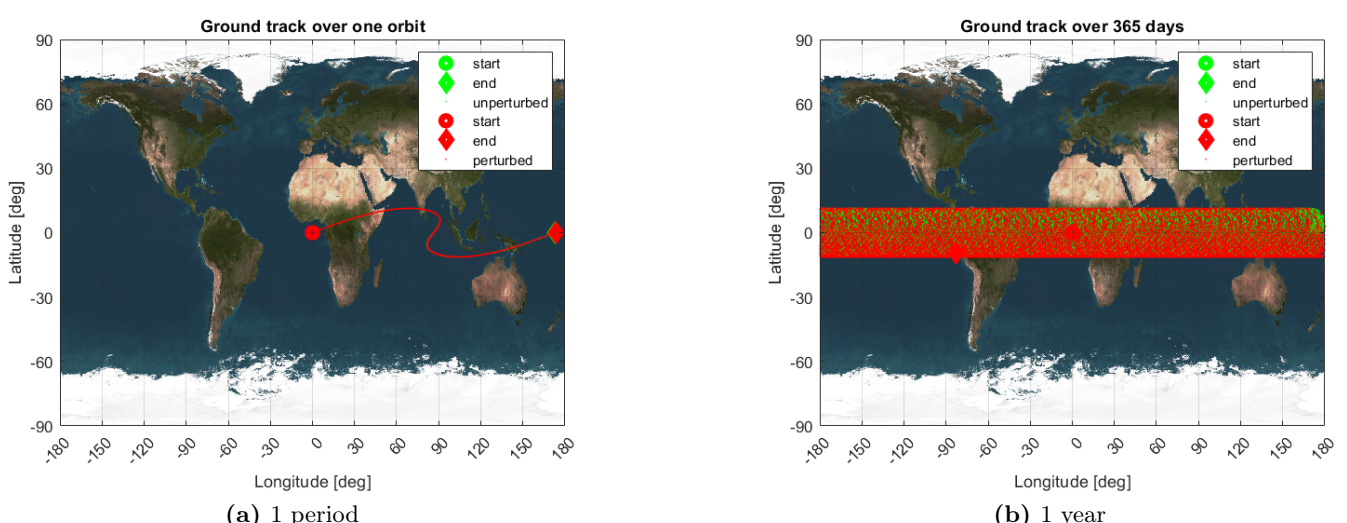
- Solar Radiation Pressure (SRP) [1]:

$$\underline{\mathbf{a}}_{\text{SRP}} = p_{\text{SR}@1\text{AU}} \left(\frac{AU}{r_{\odot \rightarrow \text{S/C}}} \right)^2 C_R \frac{A}{m} \hat{\mathbf{r}}_{\odot \rightarrow \text{S/C}} \quad (16)$$

An area-to-mass ratio $A/m = 5 \text{ m}^2/\text{kg}$ will be assumed, along with a reflectivity $C_R = 1$.

2.1 Ground track

To present a control to which the perturbed ground tracks could be compared, the ground track of the nominal orbit provided was computed using a Cartesian propagation of the trajectory and plotted over 1 period, 10 days and 1 year. On the same plot, the nominal orbit was computed and plotted under secular J2 and SRP effects. This allowed for a deeper understanding of the effects of the perturbing accelerations on the orbit of the satellite.



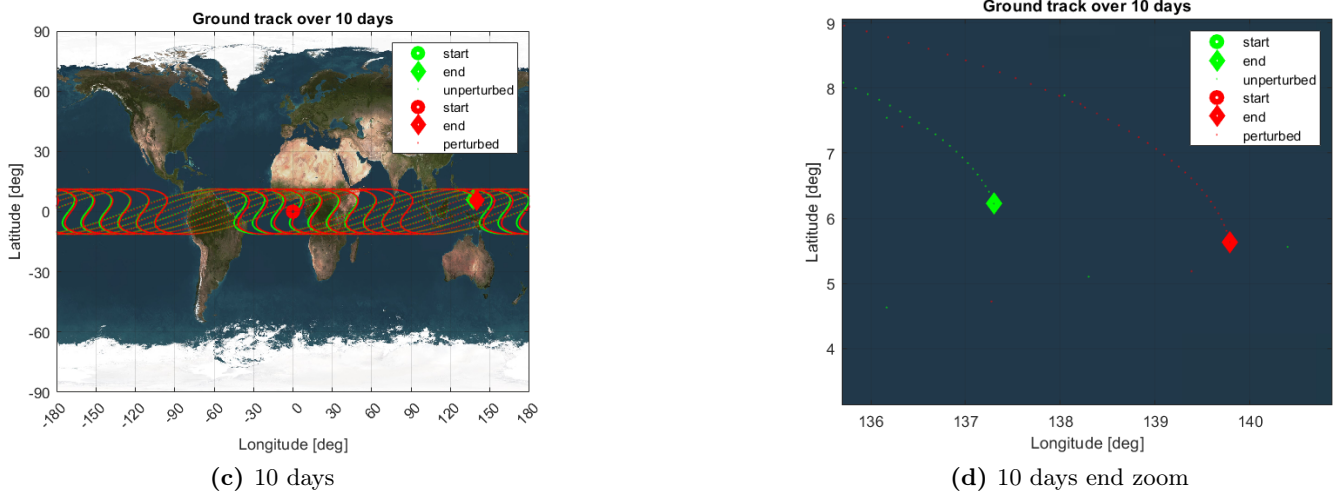


Figure 12: Unperturbed and perturbed ground tracks

2.1.1 Repeating ground track

The semi-major axis required for the repeating ground track of the satellite for the unperturbed orbit case was computed by applying the following equation [1]:

$$a = \left(\frac{\mu}{\omega_E^2} \left(\frac{m}{k} \right)^2 \right)^{1/3} \quad (17)$$

where k is the number of revolutions after which the satellite's ground track is required to repeat itself, m is the number of rotations completed by Earth in that time and ω_E the magnitude of the Earth's angular velocity respectively. For the purpose of this report, the values of k and m were required to be 2 and 1 respectively. To compute the semi-major axis corresponding to the perturbed satellite motion, J2 effects equations were implemented in MATLAB as anonymous functions making possible the evaluation of the following implicit equation [1]:

$$\frac{m}{k} = \frac{(\omega_E - \dot{\Omega})}{(n + \dot{\omega} + M_o)} \quad (18)$$

where n stands for the mean motion of the satellite. Finally, a convergent solution to Equation 18 was found by using MATLAB `fzero.m` function and the semi-major axis of the orbit required for the repeating ground track was computed. The ground track of this orbit was computed and plotted in the same way as that of the nominal orbit. The new semi-major axis to obtain an unperturbed satellite's repeating ground track is estimated to be 26560.413 km. The ground track repeats almost exactly in the case of unperturbed orbit. However, this is not true for the perturbed case. This could be explained by the fact that in the case where secular J2 and SRP effects are accounted for, some of the orbital elements vary with time, affecting in this way the longitude and latitude values as

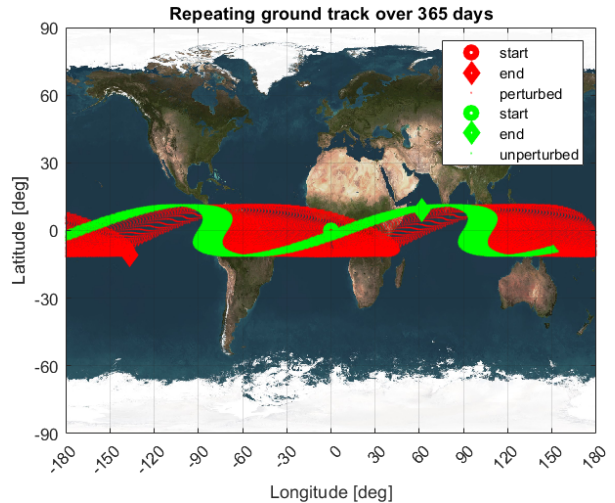


Figure 13: Repeating ground track over 1 year



well. In addition, the numerical approximation scheme (i.e. Runge-Kutta) employed to integrate the perturbing acceleration term, might require more time steps to improve its fidelity.

2.2 Orbit propagation

For propagating the initial orbit and hence determine the corresponding time-evolution of the orbital elements, two different approaches will be implemented and compared:

- Cartesian coordinates propagation [1]:

$$\text{solve } \ddot{\mathbf{r}} = -\frac{\mu}{r^3} \mathbf{r} + \mathbf{a}_{\text{pert}} \xrightarrow{\text{car2kep}} \underbrace{\{a, e, i, \Omega, \omega, \theta\}}_{:=\underline{\alpha}(t)} \quad \forall t \quad (19)$$

- Gauss planetary equations [1]:

$$\begin{aligned} \mathbf{a}_{\text{pert}}^{(\text{tnh})} &= [\hat{\mathbf{t}} | \hat{\mathbf{n}} | \hat{\mathbf{h}}]^\top \mathbf{a}_{\text{pert}}^{(\text{cart})} \\ \text{solve } &\left\{ \begin{array}{l} \dot{a} = (\dots) \\ \dot{e} = (\dots) \\ \vdots \\ \dot{\theta} = (\dots) \end{array} \right. \quad \underline{\alpha}(t) \quad \forall t \end{aligned} \quad (20)$$

It can be experienced that, for a given tolerance assigned to the ODE solver, there is a very small difference in terms of accuracy between the two methods. This may for instance be proved by computing the error relative to the time evolution obtained for each element. Propagating the initial conditions for 1 year and setting Relative Tolerance = 10^{-12} , Absolute Tolerance = 10^{-15} yields for instance:

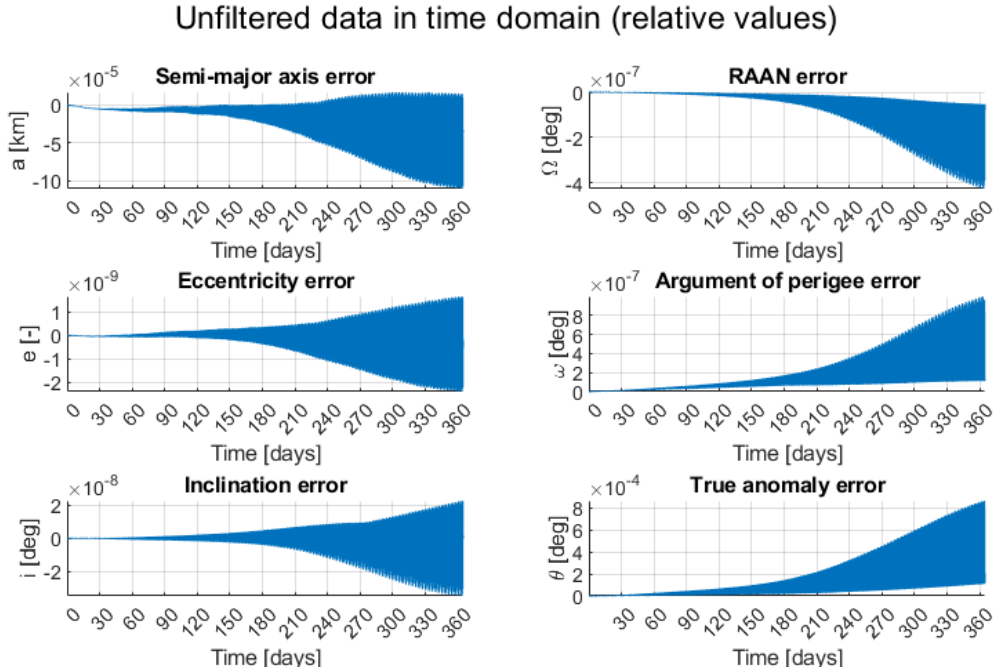


Figure 14: Differences between Cartesian and Gaussian propagation

Such values are relatively close to round-off errors, which indeed confirms our initial statement. A difference may instead be highlighted in terms of computational efficiency, as shown in Figure 15: Gauss planetary equations are about twice as quick as Cartesian coordinates integration.



The Keplerian elements were computed over a period of 1 year, sufficient to show their periodic evolution due to both SRP and J2 perturbations. The number of time steps was chosen to be 21024, one each 25 minutes or $\Delta\theta = 12^\circ$, a number which gave good accuracy and a reasonable computational time when used with the ode113 solver. Each orbital element evolved differently over time, as can be seen in Figure 16. Each plot illustrates a periodic (non-secular) and non-periodic (secular) effect by the perturbations on each element except true anomaly. Figure 17b shows how the orbit's shape and orientation would change throughout the S/C life-cycle, provided that no orbit maintenance maneuver is performed.

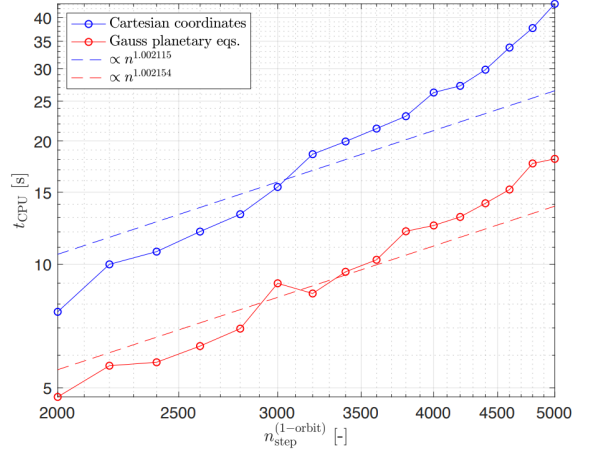


Figure 15: Computational efficiencies

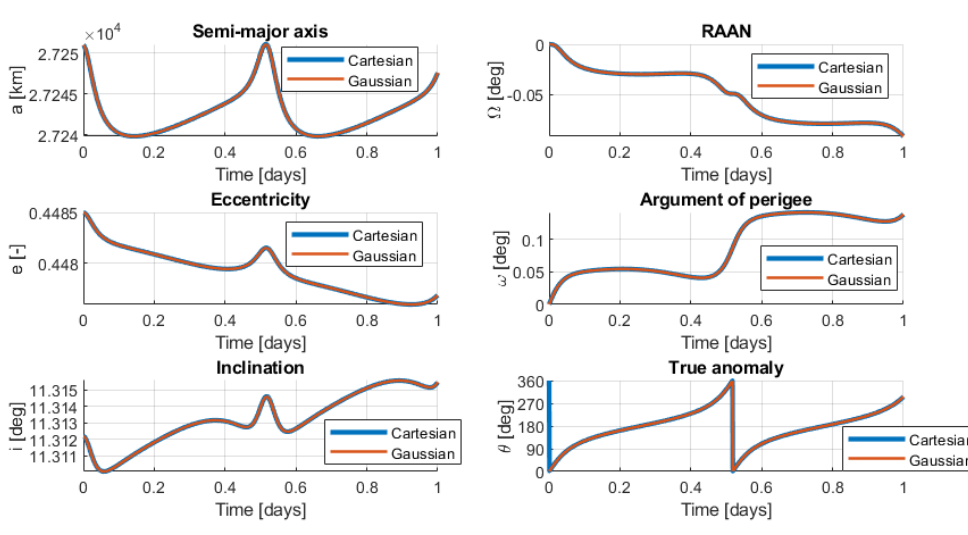
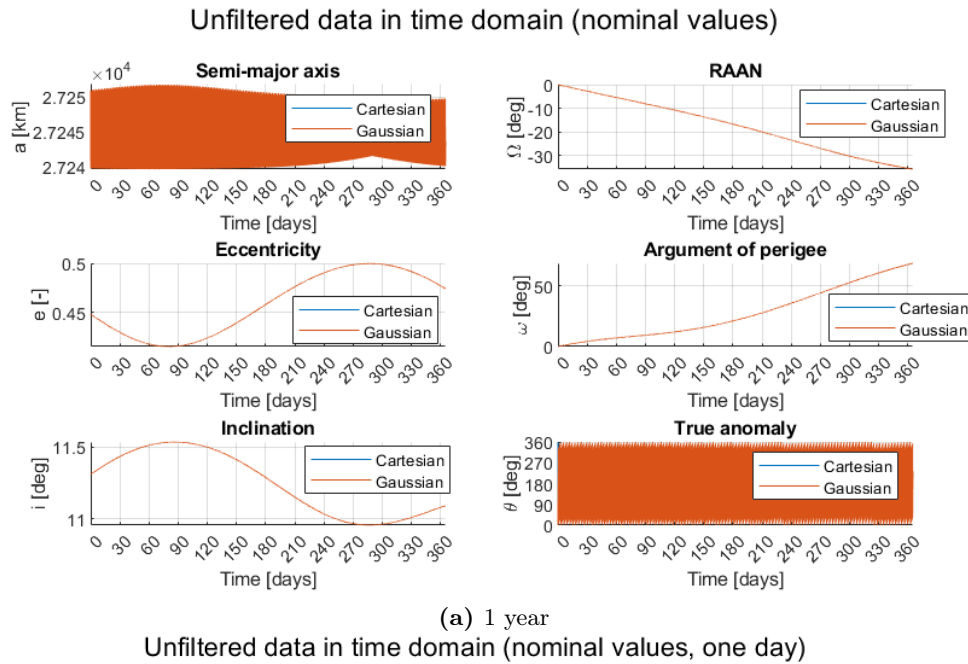


Figure 16: Orbit propagation



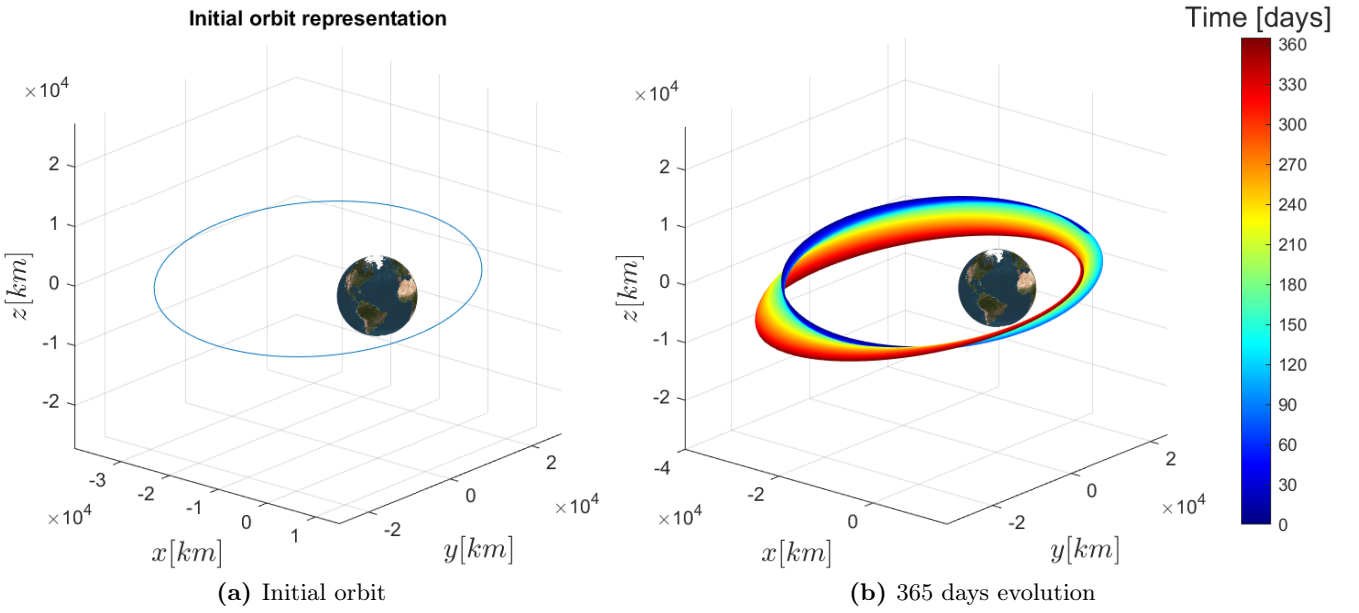


Figure 17: Nominal orbit

2.3 Filtering of high frequencies

In order to understand the physical meaning of the oscillations in the evolution of the Keplerian elements, the frequency spectrum needed to be studied. To do so, the elements underwent a discrete Fourier transform, of which only the amplitude was analyzed. Having used a Fast Fourier Transform (FFT) algorithm set, the result is a complex number that contains information on both amplitude and phase. The spectrum was plotted with a logarithmic y-axis to obtain a clear visualization of the data and so as not to have the plot dominated by the amplitude associated to the zero frequency.

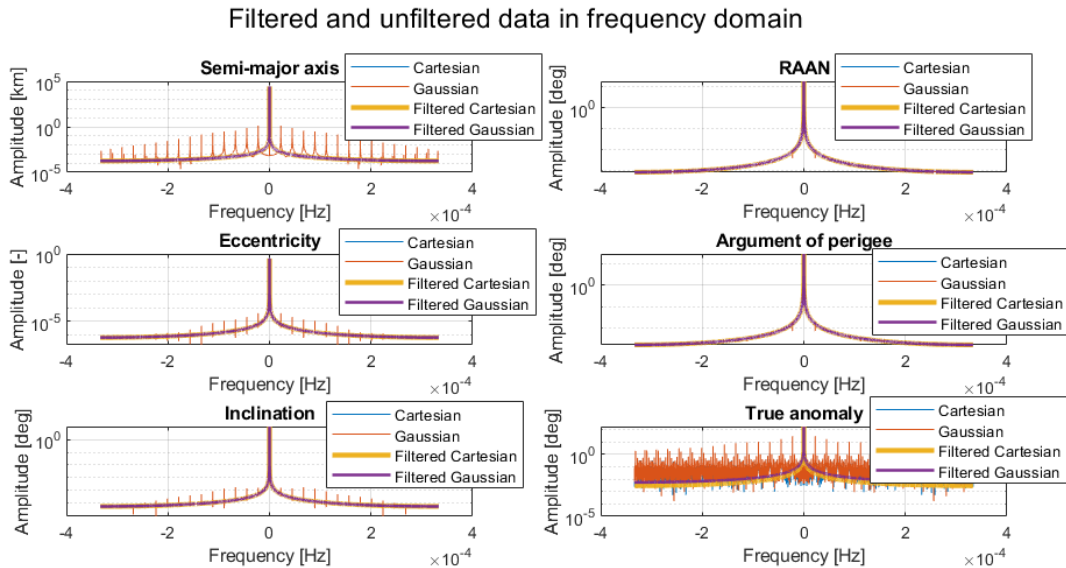


Figure 18: Keplerian parameters oscillation frequency spectrum

As Figure 18 shows, five out of six of the unfiltered signals peaks are within the $(-4 * 10^{-4} \text{ Hz}, 4 * 10^{-4} \text{ Hz})$ band, with semimajor axis, eccentricity and inclination which have higher amplitude variation (a phenomenon present in the time domain, too) than RAAN and perigee anomaly,



which have a stepped and linear-like (ramp) trend. In order to retrieve the secular evolution of the Keplerian elements, the aforementioned short-term oscillations must be filtered out. As these oscillations were associated with higher frequencies, a symmetric Moving Average Filter (MAF) has been chosen to perform the filtering. One drawback of the MAF is that when close to the extremes of the domain, the filtered signal will drift toward the unfiltered signal, until matching at the most extreme point. This is due to how the MAF works, as the filtered value of any given point is computed as the average of the $N/2-1$ points that follow and the $N/2-1$ points that come before. When close to the extremes, there might be less than $N/2-1$ points to the left or to the right of the point to filter. Thus the choice of width of the averaging window is a trade-off: increasing the number of points provides a smoother solution, but a less accurate result at the extremes of the domain. The results below were obtained with a window width of 700 points, approximately one for each orbit completed by the S/C in 1 year.

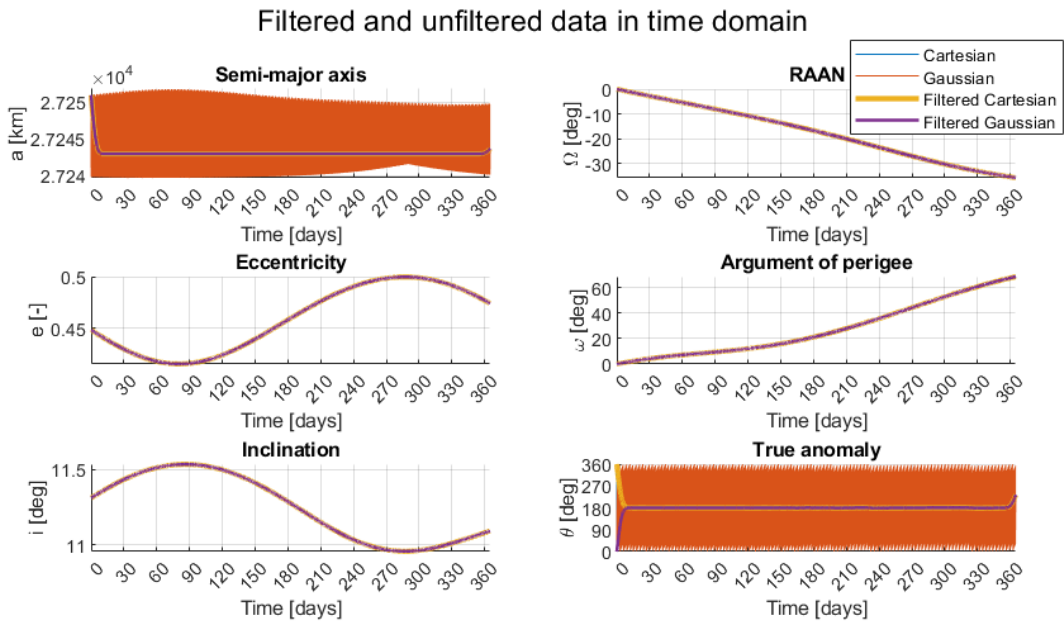


Figure 19: Filtered orbit propagation

Figure 19 shows the filtered 1 year Keplerian elements evolution: it is a straight line, except at the extremes due to the aforementioned reasons. The straight line display the secular effects which affect the Keplerian elements. The moving average filter makes clear that the Keplerian elements' trend in frequency domain is similar to a parabola, as expected as the filtered time variation of the Keplerian elements is a straight line, given the nature of the Fourier transformation.

2.4 Comparison with real data

In order to validate the numerical propagation, a comparison with the results produced by the NASA HORIZONS propagator [2] has been made for the BREEZE-M R/B satellite (NORAD 34942), chosen after querying *space-track* [3] with Keplerian elements similar to the given mission requirements. In Figure 20 the orbital elements evolution obtained by HORIZONS has been plotted against the results obtained propagating the same initial orbital elements with our model.

Table 13: BREEZE-M R/B satellite (NORAD 34942) query result and initial orbital elements

a	e	i	Ω	ω	θ
24856 km	0.4276	9.44°	-	-	-
31235 km	0.3445	10.1218°	3.7652°	123.4424°	343.0054°



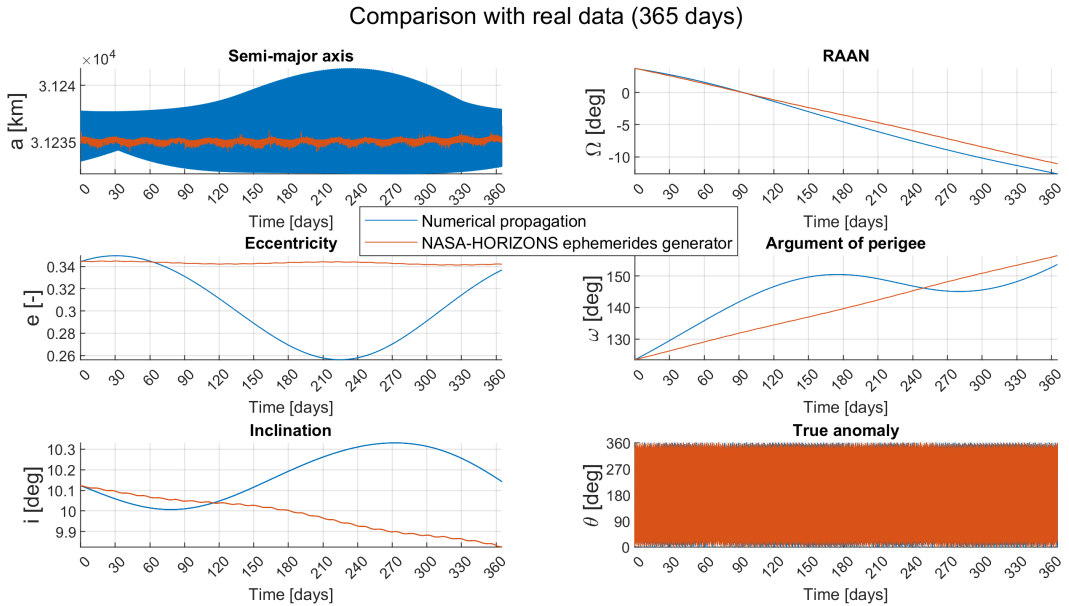


Figure 20: Comparison between HORIZONS and numerical method Keplerian elements evolution

The results are very good for Ω and sufficient for a and ω , while there are considerable differences in e and i evolution. These differences between the obtained plots occur due to the fact that only 2 perturbations were modelled for the numerical propagation (J2 and SRP). In reality, the orbital elements are influenced by many other perturbing accelerations. These include the gravitational acceleration due to the Moon, atmospheric drag, the influence of Earth's magnetic field and the gravitational acceleration due to other planets in the solar system. For example, in Figure 21 it's shown that in the HORIZONS propagation plot there is a 14 days (half the revolution period of the Moon around Earth) periodic oscillation absent in the numerical propagation. This happens due to neglect of Moon's third body perturbing effect in our model. Accounting for it translates also into considerable long term variations.

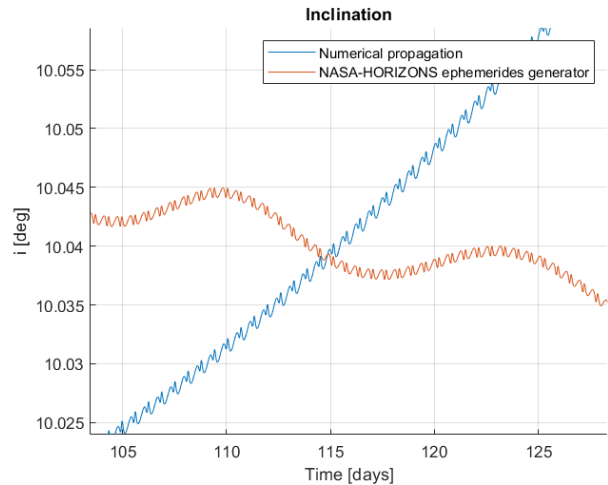


Figure 21: i detail in the comparison with real data

References

- [1] Howard Curtis. *Orbital Mechanics for Engineering Students, 4th Edition*. Butterworth-Heinemann, 2020.
- [2] NASA - National Aeronautics and Space Administration. *Horizons System*.
- [3] SAIC - Science Applications International Corporation. space-track.org.